

# Excited State Mean-Field Theory without Automatic Differentiation

Luning Zhao<sup>1</sup> and Eric Neuscamman<sup>2,3, a)</sup>

<sup>1)</sup>*Department of Chemistry, University of Washington, Seattle, Washington 98195, USA*

<sup>2)</sup>*Department of Chemistry, University of California, Berkeley, California 94720, USA*

<sup>3)</sup>*Chemical Sciences Division, Lawrence Berkeley National Laboratory, Berkeley, CA, 94720, USA*

(Dated: 21 December 2024)

We present a formulation of excited state mean-field theory in which the derivatives needed for wave function optimization are expressed analytically in terms of a collection of Fock-like matrices. By avoiding the use of automatic differentiation and grouping Fock builds together, we find that the number of times we must access the memory-intensive two-electron integrals can be greatly reduced. Furthermore, the new formulation allows the theory to exploit existing strategies for efficient Fock matrix construction. We demonstrate this advantage explicitly via the shell pair screening strategy, which allows us to examine the theory’s predictions for charge-redistribution during a charge transfer excitation between minimally-solvated Li and F atoms. Using coupled cluster as a benchmark, we find that the theory successfully captures the orbital relaxation effects that are missing in time-dependent density functional theory while avoiding the self-interaction-induced over-delocalization seen in unrestricted and restricted-open-shell Kohn Sham theory.

## I. INTRODUCTION

Whether one is talking about light harvesting,<sup>1,2</sup> photocatalysts,<sup>3,4</sup> core spectroscopy,<sup>5–7</sup> metal-to-ligand charge transfer,<sup>8,9</sup> or non-adiabatic dynamics,<sup>10,11</sup> reliable predictions of excited state properties are extremely valuable. However, the leading theoretical methods for modeling excited states are fundamentally more approximate than their ground state counterparts due to their reliance on additional approximations. Linear response (LR) methods, for example, assume that the excited state is in some way close to the ground state in state space, leading in practice to a situation in which crucial orbital relaxation effects<sup>12–15</sup> are simply absent in configuration interaction singles (CIS)<sup>16</sup> and time-dependent density functional theory (TDDFT)<sup>16–18</sup> and only treated in a limited manner in singles and doubles equation-of-motion Coupled Cluster (EOM-CCSD) theory.<sup>19</sup> These shortcomings contribute to the difficulties that CIS and TDDFT have with charge transfer (CT) states<sup>13,15</sup> and to the eV-sized errors that EOM-CCSD often makes for doubly excited states.<sup>20,21</sup> As these difficulties arise in part from a lack of orbital relaxation following an excitation, the development of excited state methods that have fully-relaxed, excited-state-specific orbitals is strongly desirable.

Towards this end, the recently-introduced excited state mean-field (ESMF) theory<sup>22</sup> attempts to provide a minimally-correlated reference state for single excitations in which the orbitals are fully relaxed. In some aspects, ESMF is similar to the  $\Delta$ SCF approach<sup>23–26</sup> and the restricted open-shell Kohn Sham (ROKS) approach,<sup>27,28</sup> but in contrast to these methods it delivers a completely spin-pure wave function by construction and can handle states in which multiple singly-excited configurations are present in a superposition. However, like Hartree-Fock (HF) theory,<sup>29,30</sup> the accuracy of ESMF itself is limited by its lack of correlation effects, and so recent

work has studied its value as a foundation for both perturbation theory<sup>31</sup> and a novel form of density functional theory.<sup>15</sup> The perturbation theory results are particularly exciting, with preliminary testing showing an accuracy that exceeds that of EOM-CCSD.<sup>31</sup>

Like  $\sigma$ -SCF<sup>32,33</sup> and some quantum Monte Carlo approaches to excited states,<sup>21,34–36</sup> ESMF takes a variational approach to orbital relaxation in which it minimizes a function whose global minimum is the desired excited state. However, unlike these approaches, the generalized variational principle (GVP) that ESMF minimizes is defined in terms of the norm of the energy gradient,<sup>31</sup> and so the optimization requires some information about second derivatives of the energy with respect to the wave function variables. On the bright side, automatic differentiation (AD) via TensorFlow<sup>37</sup> or any other general-purpose AD framework can be employed to evaluate the necessary derivatives while maintaining the same Fock-matrix-build cost-scaling of an ESMF energy evaluation. On a less positive note, this approach requires the memory-intensive two-electron integrals (TEIs) to be accessed many times during each evaluation of the GVP’s gradient and makes it difficult to take advantage of acceleration techniques like shell-pair screening,<sup>38</sup> density fitting,<sup>39</sup> and tensor hyper contraction.<sup>40–42</sup> Thus, while AD has been extremely helpful in quickly developing an initial implementation for testing ESMF theory (see Appendix for examples of cumbersome expressions that it allows one to avoid), it severely limits the practical efficiency of the approach. In this study, we develop explicit analytic expressions for the objective function’s gradient that simplify into a collection of nine Fock-like matrix builds that can be carried out together (thus minimizing the number of times the TEIs need to be accessed) and which can benefit straightforwardly from acceleration methods. The result is a dramatic speedup compared to our previous TensorFlow implementation, thus allowing ESMF theory to be used in significantly larger systems.

We will begin with a brief review of ESMF theory, including the wave function ansatz and the GVP employed in its optimization. We will then discuss why the TensorFlow

<sup>a)</sup>Electronic mail: eneuscamman@berkeley.edu.

implementation of the energy derivatives is inefficient, after which we derive the analytic energy derivative expressions and show how they can be formulated using Fock-builds. Following these theoretical developments, we test the efficiency in two charge-transfer systems and demonstrate a speedup of two orders of magnitude relative to our previous implementation. We then turn to an investigation of charge transfer in a minimally-solvated environment that would not have been possible with the previous AD-based approach to evaluating the GVP derivatives. Finally, we conclude with a summary and some comments on future directions.

## II. THEORY

### A. ESMF Method

In ESMF, the wave function ansatz is written as

$$|\Psi\rangle = e^{\hat{X}} \left( c_0 |\Phi\rangle + \sum_{ia} \sigma_{ia} \hat{a}_{a\alpha}^\dagger \hat{a}_{i\alpha} |\Phi\rangle + \tau_{ia} \hat{a}_{a\beta}^\dagger \hat{a}_{i\beta} |\Phi\rangle \right) \quad (1)$$

in which  $|\Phi\rangle$  is the restricted Hartree-Fock determinant, and the coefficients  $\sigma_{ia}$  and  $\tau_{ia}$  correspond to excitations of an alpha-spin and a beta-spin electron, from the  $i$ th occupied orbital to the  $a$ th virtual orbital. The operator  $\hat{X}$  is defined as,

$$\hat{X} = \sum_{pq} X_{pq} \hat{a}_p^\dagger \hat{a}_q \quad (2)$$

in which  $X$  is an anti-symmetric matrix so that the orbital rotation operator  $\hat{U} = \exp(\hat{X})$  is unitary. Although there is an argument to be made that a single open-shell configuration state function should be seen as the minimally correlated reference function for excited states, we choose to include all singly-excited configurations in order to handle states in which two or more of these configurations exist in a superposition, as for example occurs in the low-energy spectrum of  $N_2$ . Although such states are technically multi-configurational, they certainly do not require a general-purpose strongly correlated ansatz and indeed are already treated at a qualitatively correct level by CIS. That said, the open shell character of ESMF (in which two electrons correlate their positions so as to not reside in the same spatial orbital simultaneously) does involve more correlation than HF theory and so it is a step further away from a true mean-field theory in which no correlation is present at all.

In the initial development of ESMF theory,<sup>22</sup> the ansatz was optimized using the Lagrangian

$$L_{\tilde{\lambda}} = W + \tilde{\lambda} \cdot \nabla E \quad (3)$$

in which  $W$  was seen as an approximated excited state variational principle whose purpose is to guide the optimization to the energy stationary point associated with a particular excited state and  $\tilde{\lambda}$  is a set of Lagrange multipliers that ensure that the optimized wave function is indeed an energy stationary point. The approximate variational principle was chosen as

$$W = (\omega - E)^2 \approx \frac{\langle \Psi | (\omega - H)^2 | \Psi \rangle}{\langle \Psi | \Psi \rangle} \quad (4)$$

which, although successful in initial testing on small molecules, was found to have multiple shortcomings. First, the target function is not bounded from below with respect to Lagrangian multipliers, making simple quasi-Newton methods difficult to use directly. Instead, the expression  $|\nabla L_{\tilde{\lambda}}|^2$  was minimized, which further increased the computational cost by necessitating an additional layer of automatic differentiation (still the right cost scaling, but now containing components that formally involve triple derivatives of the energy). Further, a more recent study<sup>31</sup> found that this approach can show poor numerical conditioning, sometimes requiring hundreds of quasi-Newton iterations to converge.

In order to address these two problems, a finite-difference Newton-Raphson (NR) method was developed for an objective function based not on Lagrange multipliers but instead on a GVP.<sup>31</sup>

$$L_{\mu\chi} = \chi \left( \mu (\omega - E)^2 + (1 - \mu) |\nabla E|^2 \right) + (1 - \chi) E \quad (5)$$

Starting with  $\chi$  set to 1,  $\mu$  is gradually reduced to zero during the optimization so as to ensure convergence to the stationary point with energy closest to  $\omega$ . Unlike the target function in Equation 3, this approach is bounded from below, allowing both NR and quasi-Newton methods to be employed without the need for an additional layer of AD. In addition, one can switch  $\chi$  to 0 close to convergence and rely on stationary-point methods like NR, thus potentially benefiting from even more efficient gradients and such method's super-linear convergence. In practice, initial testing has shown this approach to be more robust and more efficient than Equation 3 in a variety of systems.<sup>31</sup>

### B. Analytical Derivatives

Even though this new approach improved the optimization's efficiency, its implementation still relied on AD for the derivatives of both the energy and  $L_{\mu\chi}$ , which, although convenient, leads to an unnecessarily high prefactor in the method's cost due to frequent access of the TEIs and the handling of the TEIs as a dense 4-index array without the efficiencies that accelerated Fock-build methods enjoy. In order to address this source of inefficiency, we will now derive explicit expressions for the analytical derivatives of the ESMF energy and objective function and show that they can be formulated as a set of Fock matrix builds. We will focus on the special case of singlet excited states, whose wave function can be written as

$$|\Psi\rangle = e^{\hat{X}} \left( c_0 |\Phi\rangle + \sum_{ia} \sigma_{ia} \left( \hat{a}_{a\alpha}^\dagger \hat{a}_{i\alpha} + \hat{a}_{a\beta}^\dagger \hat{a}_{i\beta} \right) |\Phi\rangle \right) \quad (6)$$

in which the alpha and beta electron excitations have the same coefficients. Although the derivation will be based on singlet excited states, a generalization to the triplet case is straightforward.

TABLE I: Summary of Notation

Description	Notation
One-electron Integrals	$\mathbf{G}$
Two-electron Integrals	$(pq rs)$
RHF Determinant Coefficient	$c_0$
Excited Determinant Coefficient	$\sigma$
Unitary Orbital Rotation	$\mathbf{U}$
$c_0$ Lagrangian Multiplier	$\mu_0$
$\sigma$ Lagrangian Multiplier	$\mu$
$U$ Lagrangian Multiplier	$\mathbf{M}$
First $N_o$ Rows of $\mathbf{U}$	$\Theta$
Last $N_v$ Rows of $\mathbf{U}$	$\Gamma$
First $N_o$ Rows of $\mathbf{M}$	$\mathbf{R}$
Last $N_v$ Rows of $\mathbf{M}$	$\Phi$
General Fock Matrix	$\mathbf{F}[\mathbf{D}]$
Wave Function Square Norm	$N_2 = c_0^2 + 2 \sum_{ia} c_{ia}^2$
$\mathbf{A}$ Matrix	$\Gamma^T \sigma^T \sigma \Gamma - \Theta^T \sigma \sigma^T \Theta$
$\mathbf{B}$ Matrix	$\Theta^T \sigma^T \sigma \Gamma - \mathbf{R}^T \sigma \sigma^T \Theta$
Matrix Trace	$\text{Tr}[\mathbf{O}] = \sum_p O_{pp}$
Matrix Inner Product	$\mathbf{O} \cdot \mathbf{V} = \sum_{pq} O_{pq} V_{pq}$

### 1. Notation

Before we derive ESMF energy, target function, and derivatives, we introduce the notations used in our derivations. Orbital index  $i, j, k$  denote occupied canonical orbitals from restricted HF (RHF), and index  $a, b, c$  denote the corresponding virtual orbitals. We use the indices  $p, q, r, s$  for general orbitals. We denote the first  $N_o$  rows of the  $\mathbf{U}$  matrix as  $\Theta$ , where  $N_o$  is the total number of occupied orbitals. The last  $N_v$  rows of  $\mathbf{U}$  are denoted as the matrix  $\Gamma$ , where  $N_v$  is the number of virtual orbitals. Similarly, we denote the corresponding blocks of the matrix  $\mathbf{M}$  (see Table I) as  $\mathbf{R}$  and  $\Phi$ .

We define the “generalized” Coulomb, exchange, and Fock matrices as,

$$\begin{aligned}
 J[\mathbf{D}]_{pq} &= \sum_{rs} D_{rs} (rs|pq) \\
 K[\mathbf{D}]_{pq} &= \sum_{rs} D_{rs} (pr|qs) \\
 F[\mathbf{D}]_{pq} &= 2J[\mathbf{D}]_{pq} - K[\mathbf{D}]_{pq}
 \end{aligned} \tag{7}$$

in which  $(rs|pq)$  are the two-electron integrals in the RHF canonical orbital basis in 1122 order, and  $\mathbf{D}$  is a “generalized” density matrix which is not necessarily symmetric. For a summary of the notation for the scalar and matrix quantities we use, as well as for some matrix operations, see Table I.

### 2. ESMF Energy

The ESMF energy can be formulated as

$$E = \frac{E_1 + E_2}{N_2} \tag{8}$$

in which the one- and two-body components are

$$\begin{aligned}
 E_1 &= 2N_2 \text{Tr}[\Theta \mathbf{G} \Theta^T] + 4c_0 \text{Tr}[\Theta \mathbf{G} \Gamma^T \sigma^T] \\
 &\quad + 2 \text{Tr}[\sigma \Gamma \mathbf{G} \Gamma^T \sigma^T - \Theta \mathbf{G} \Theta^T \sigma \sigma^T]
 \end{aligned} \tag{9}$$

and

$$\begin{aligned}
 E_2 &= 2N_2 \mathbf{F}[\Theta^T \Theta] \cdot (\Theta^T \Theta) + 4c_0 \mathbf{F}[\Theta^T \Theta] \cdot (\Theta^T \sigma \Gamma) \\
 &\quad + 2 \mathbf{F}[\Theta^T \Theta] \cdot \mathbf{A} + 2 \mathbf{F}[\Theta^T \sigma \Gamma] \cdot (\Theta^T \Theta)
 \end{aligned} \tag{10}$$

respectively. These expressions reveal that the most expensive part of the ESMF energy is the construction of two Fock matrices:  $\mathbf{F}[\Theta^T \Theta]$  and  $\mathbf{F}[\Theta^T \sigma \Gamma]$ . Note that this is different from HF theory, in which only one Fock matrix,  $\mathbf{F}[\Theta^T \Theta]$ , is needed to evaluate the energy. In fact, we note that if we set  $\sigma = \mathbf{0}$ , then the ESMF energy becomes the HF energy expression.

### 3. Lagrangian Derivatives

Starting from the energy, we have derived the first derivatives  $\partial E / \partial c_0$ ,  $\partial E / \partial \sigma$ ,  $\partial E / \partial \Theta$ , and  $\partial E / \partial \Gamma$ , detailed expressions for which can be found in the Appendix. Note that these derivatives require the construction of one additional Fock matrix,  $\mathbf{F}[\mathbf{A}]$ , in addition to the two required for the energy itself. In order to use these derivatives in an ESMF optimization, we consider first the Lagrangian multiplier approach of Equation 3, after which we show that the derivatives of the newer target function in Equation 4 can be evaluated in the same way by plugging a particular set of values into the Lagrangian multipliers.

We first expand the Lagrange multiplier dot product as

$$L_{\vec{\lambda}} = W + \mu_0 \frac{\partial E}{\partial c_0} + \sum_{ia} \mu_{ia} \frac{\partial E}{\partial \sigma_{ia}} + \sum_{pq} M_{pq} \frac{\partial E}{\partial X_{pq}} \tag{11}$$

and note that the derivative of  $W$  with respect to any variable  $x$  are simple once the energy first derivatives have been evaluated.

$$\frac{\partial W}{\partial x} = -2(\omega - E) \frac{\partial E}{\partial x} \tag{12}$$

Noting that the remaining part of  $L$  can be written in terms of the auxiliary quantities  $L_1$ ,  $L_2$ , and  $L_3$  (defined in the Appendix), the target function becomes

$$\begin{aligned}
 L &= W + (\mu_0 L_1 - 2\mu_0 E c_0) / N_2 \\
 &\quad + \left( L_2 - 4E \sum_{ia} \sigma_{ia} \mu_{ia} \right) / N_2 + L_3 / N_2.
 \end{aligned} \tag{13}$$

Inspecting the definition of  $L_3$ , we find that this approach requires two additional Fock builds:  $\mathbf{F}[\mathbf{R}^T \Theta]$  and  $\mathbf{F}[\mathbf{R}^T \sigma \Gamma]$ , bringing us to five total Fock builds for this approach to constructing the energy, its derivatives, and  $L$ .

Although we again relegate the details to the Appendix, we find that evaluating the derivatives of  $L_1$ ,  $L_2$ , and  $L_3$  with respect to  $c_0$ ,  $\sigma$ ,  $\Theta$ , and  $\Gamma$  requires another four Fock builds:  $\mathbf{F}[\Theta^T \mu \Gamma]$ ,  $\mathbf{F}[\Theta^T \sigma \Phi]$ ,  $\mathbf{F}[\Theta^T \mu \sigma^T \Theta]$ , and  $\mathbf{F}[\mathbf{B}]$ . Thus, after constructing a total of nine Fock-like matrices, the evaluation of the derivatives of  $L$  with respect to all of the ESMF wave function variables amounts to an inexpensive (relative to the Fock builds) collection of operations on matrices whose dimensions are no worse than the number of orbitals.

At this point, two details are worth addressing. First, the above derivation uses one- and two-electron integrals defined in the RHF canonical molecular orbital basis. Were we to actually form the TEI tensor in this basis, we would incur the standard  $O(N^5)$  cost scaling of the integral transformation, which would immediately replace the Fock builds as the leading term in the method's asymptotic cost scaling. Instead, we note that expensive integral transformations can be avoided because the only place in the theory that the TEIs are used is in the Fock builds. Therefore, instead of transforming the two-electron integrals, we can apply the orbital rotation to each of the nine density matrices that are fed in to the Fock build, thus allowing us to keep the TEIs in the atomic orbital basis.

Second, we have so far derived derivatives with respect to the elements of  $\mathbf{U}$ , but the actual orbital rotation parameters are the elements of  $\mathbf{X}$ . To get all the way to derivatives with respect to  $\mathbf{X}$ , there are at least two possible routes. On the one hand, AD (e.g. via TensorFlow) can be used to complete the last step in a reverse-accumulation approach, in which the values for  $\partial E / \partial \mathbf{U}$  that we have calculated via our analytic expression are fed in to reverse accumulation through the matrix exponential function. On the other hand, if we wish to strictly avoid AD (although for this part of the evaluation there is not such a clear efficiency case for doing so) we can instead rederive our orbital rotation matrix as

$$\mathbf{U} \rightarrow \tilde{\mathbf{U}} \exp(\mathbf{X}) \quad (14)$$

where after each optimization step we reset  $\mathbf{X}$  to zero by absorbing its rotation into  $\tilde{\mathbf{U}}$  and then exploiting the simple relationship  $\exp(\mathbf{X}) = \mathbf{1} + \mathbf{X}$ . Either way, once we have evaluated the energy derivatives with respect to  $\mathbf{U}$ , converting them to derivatives with respect to  $\mathbf{X}$  is inexpensive compared to the Fock builds.

#### 4. GVP Derivatives

We now turn to the derivatives of Equation 5 with respect to some wave function variable  $x$ .

$$\begin{aligned} \frac{\partial L_{\mu\chi}}{\partial x} = & \chi \left( -2\mu(\omega - E) \frac{\partial E}{\partial x} + 2(1 - \mu) \sum_y \frac{\partial E}{\partial y} \frac{\partial^2 E}{\partial x \partial y} \right) \\ & + (1 - \chi) \frac{\partial E}{\partial x} \end{aligned} \quad (15)$$

Now, compare this expression to the derivatives of  $L_{\tilde{\lambda}}$ .

$$\frac{\partial L_{\tilde{\lambda}}}{\partial x} = -2(\omega - W) \frac{\partial E}{\partial x} + \sum_y \lambda_y \frac{\partial^2 E}{\partial x \partial y} \quad (16)$$

If we first evaluate the energy derivatives, which requires three Fock builds, we can replace the Lagrange multipliers in Eq. (16) with these energy derivatives, at which point the approach discussed above for evaluating the derivatives of  $L_{\tilde{\lambda}}$  can be used for evaluating the term inside the large parentheses in Eq. (15). Thus, as for the Lagrange multiplier objective function,

the GVP objective function's derivatives can be evaluated at the cost of nine Fock builds (the three already done for the energy derivatives plus the remaining six).

#### C. Shell-Pair Screening

In total, our analytic evaluation of the derivatives needed for ESMF optimization requires building nine Fock matrices.

- |   |   |
|---|---|
| 1. $\mathbf{F}[\Theta^T \Theta]$            | 6. $\mathbf{F}[\Theta^T \mu \Gamma]$          |
| 2. $\mathbf{F}[\Theta^T \sigma \Gamma]$     | 7. $\mathbf{F}[\Theta^T \sigma \Phi]$         |
| 3. $\mathbf{F}[\mathbf{A}]$                 | 8. $\mathbf{F}[\Theta^T \mu \sigma^T \Theta]$ |
| 4. $\mathbf{F}[\mathbf{R}^T \Theta]$        | 9. $\mathbf{F}[\mathbf{B}]$                   |
| 5. $\mathbf{F}[\mathbf{R}^T \sigma \Gamma]$ |   |

Although this ensures that ESMF has the same asymptotic cost scaling as HF theory, it is clearly going to suffer from a higher prefactor. How to mitigate this extra cost? In this study, we employ the shell-pair screening approach to Fock matrix construction, both because it exploits sparsity in the TEIs in larger systems and because it allows us to easily group Fock builds together in order to minimize the number of times the sparse TEIs must be accessed. The shell-pair screening algorithm can be summarized as follows. At the beginning of an ESMF optimization we loop over all four indices of the two-electron integrals  $(p, q, r, s)$ , and for each index pair  $(p, q)$ , find the  $(r, s)$  index pair that maximizes the absolute value of integral  $|(pq|rs)|$ . The shell-pair  $(p, q)$  is discarded unless  $\max_{r,s} |(pq|rs)|$  is above a certain threshold, which in this work we set to  $10^{-9}$  a.u., small enough so that we achieve direct agreement with results from our older TensorFlow-based implementation. After this screening, Fock builds proceed according to Eq. (7) by looping over the retained shell-pairs. Crucially, multiple Fock matrices can be constructed during a single loop through the TEIs. As the TEIs still take up a lot of memory even after screening, it is more cache efficient to evaluate multiple fock matrices at once. Thus, when using the Lagrange multiplier objective function, we evaluate all nine Fock matrices during a single loop over the shell pairs. For the GVP objective function derivatives, we require two loops through the shell pairs, the first to evaluate the first three matrices and the second to evaluate the other six, which in that case depend on the first three due to the Lagrange multiplier values having been set equal to the energy derivatives. Finally, note that we have implemented a simple approach to shared-memory parallelism by threading the loop over shell pairs.

### III. RESULTS

#### A. Computational Details

All of the ESMF results are obtained via our own software, which extracts one- and two-electron integrals from PySCF.<sup>43</sup> The DFT, TDDFT, CIS, ROHF, and CCSD results were obtained from QChem.<sup>44</sup> We use the VESTA<sup>45</sup> software to plot

the density difference between ground and excited state. The molecular geometries can be found in the Appendix.

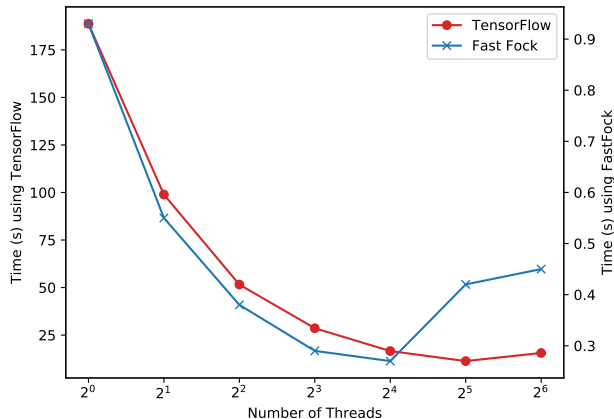


FIG. 1: Time taken to evaluate the 24 Lagrangian gradients required for inverting the Hessian during the first finite-difference NR iteration of the  $\text{Cl}^-$ - $\text{H}_2\text{O}$  optimization.

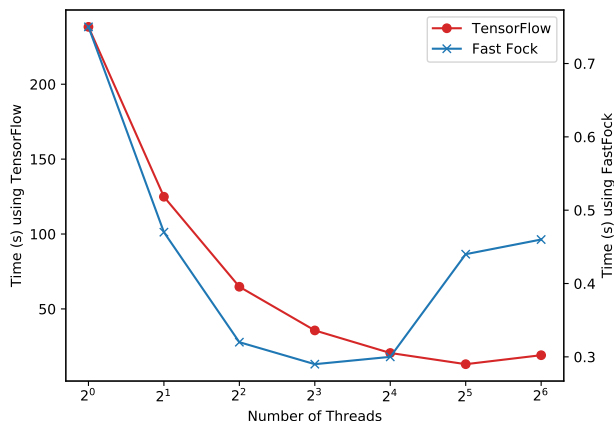


FIG. 2: Time taken to evaluate the 22 Lagrangian gradients required for inverting the Hessian during the first finite-difference NR iteration of the  $\text{NH}_3$ - $\text{F}_2$  optimization.

## B. Efficiency Gain

Here we compare the cost of two example ESMF optimizations when performed with our group’s previous AD-based implementation (denoted here as TensorFlow) with the new implementation based on analytic expressions and shell-pair screening (denoted here as FastFock). Working in the cc-pVDZ basis,<sup>46</sup> we optimize the lowest singlet charged transfer excited states of the  $\text{Cl}^-$ - $\text{H}_2\text{O}$  dimer and the  $\text{NH}_3$ - $\text{F}_2$  dimer, both of which have been studied before.<sup>15,47,48</sup> The optimization uses the finite-difference NR approach,<sup>31</sup> in which the NR

TABLE II: Excitation energies (eV) for the TensorFlow and FastFock implementations.

System	TensorFlow	Fast Fock
$\text{Cl}^-$ - $\text{H}_2\text{O}$	4.7195	4.7195
$\text{NH}_3$ - $\text{F}_2$	4.5367	4.5367

linear equation is solved via the generalized minimal residual method (GMRES), with the Hessian-vector multiplication evaluated via a simple finite difference formula involving gradients of the objective function. In Figures 1 and 2, we compare the amount of time that the two implementations took to solve the linear equation for each optimization’s first NR step. Although we would clearly need to work with larger systems for our simple multi-threading approach to saturate the 32 cores on the processor, we see a roughly 100-fold increase in speed in both cases when running 16 threads (be careful to note the different left and right axes). When run in serial, the new implementation is 202 and 314 times faster than the TensorFlow implementation for the two different systems.

In order to verify that the gain we obtained in efficiency does not come with a loss in accuracy from the shell-pair screening, we show the predicted excitation energies of  $\text{Cl}^-$ - $\text{H}_2\text{O}$  and  $\text{NH}_3$ - $\text{F}_2$  in Table II. We found that the predictions

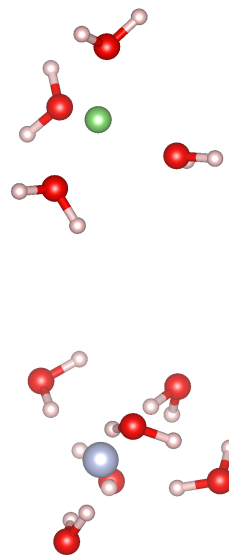


FIG. 3: The geometry of the minimally-solvated charge transfer system, in which a Li atom surrounded by four water molecules can be seen above a F atom surrounded by six water molecules. The geometry was determined by two MP2 optimizations in the 6-31G\* basis,<sup>49</sup> one for the positively-charged Li cluster in isolation and one for the negatively-charged F cluster in isolation. The two clusters were then arranged one atop the other such that the Li and F atoms were 8.05Å apart. See Appendix for the atomic coordinates.

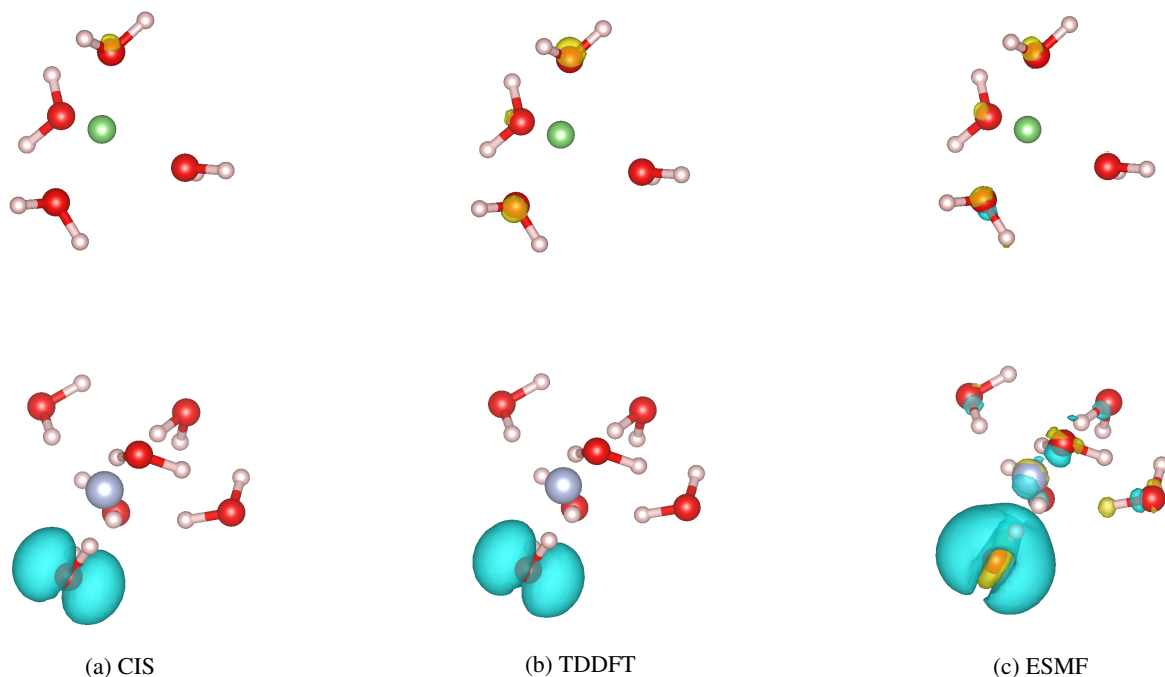


FIG. 4: Isosurface plots for the charge density changes following the charge transfer excitation that moves an electron from the lower F cluster to the upper Li cluster, with blue surfaces showing charge depletion relative to the ground state and yellow surfaces showing charge accumulation. TDDFT employed the  $\omega$ B97X functional. Note that the primary orbital on the Li cluster that accepts the transferred electron is very diffuse, and so at the isosurface value that makes charge-relaxation effects visible in the lower cluster the charge accumulation on the Li cluster is not visible. See Appendix for a plot with an isosurface value that makes the Li cluster charge accumulation more clear.

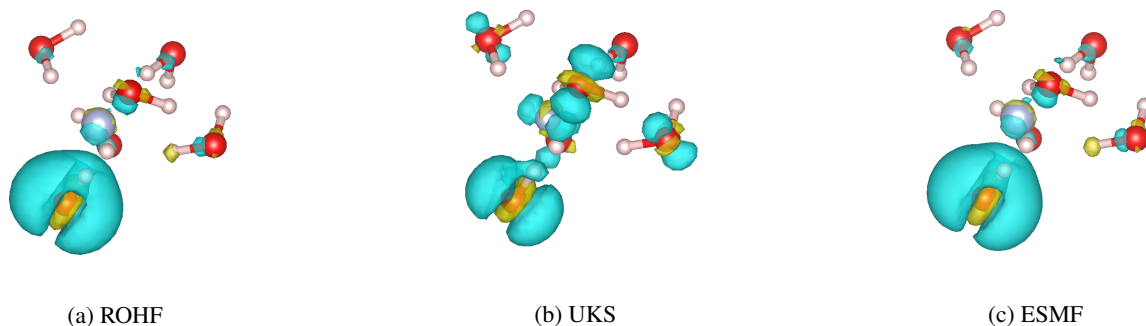


FIG. 5: As for Figure 4, but showing ROHF and UKS ground-state charge density differences between the neutral and negatively charged F cluster when modeled in isolation alongside ESMF's charge density differences when it treats the charge transfer state in the full two-cluster system. UKS employed the  $\omega$ B97X functional.

match to better than  $10^{-4}$  eV between the two implementations, indicating that there was no meaningful accuracy loss at the screening threshold we employed.

### C. Minimally-solvated charge transfer

With these efficiency improvements in hand, we are able to make an initial investigation of ESMF's predictions for how charge transfers in a minimally solvated environment. To this

purpose, we study the system shown in Figure 3, in which a Li atom and a F atom are each surrounded by a small collection of water molecules. Although the geometry optimizations used a different basis (see figure), all subsequent calculations were performed in the cc-pVDZ orbital basis. When the two clusters are simulated as a single system with ground state methods, the F and Li clusters carry negative and positive net charges, respectively. Our purpose here is to investigate the predictions that various excited state methods make for how the charge density changes in the (lowest-energy singlet)

TABLE III: Differences in atomic Mulliken populations for atoms in the lower cluster between the excited (lower cluster neutral) and ground (lower cluster negatively charged) states. For UKS, ROHF, and IP/EA-EOM-CCSD, we report the results for the corresponding charge states of the lower cluster in isolation (see text). DFT methods used the  $\omega$ B97X functional.

Method	F	O	H	H	O	H	H	O	H	H	O	H	H	O	H	H	O	H	H
CIS	0.01	0.01	0.00	0.00	0.00	0.00	0.00	0.00	0.00	0.00	0.96	0.01	0.01	0.00	0.00	0.00	0.00	0.00	0.00
TDDFT	0.01	0.00	0.00	0.00	0.00	0.00	0.00	0.00	0.00	0.00	0.96	0.01	0.01	0.00	0.00	0.00	0.00	0.00	0.00
UKS	0.06	0.04	0.00	0.02	0.11	0.01	0.03	0.10	0.03	-0.01	0.38	0.06	0.05	0.03	-0.01	0.01	0.08	0.01	0.03
ROKS	0.03	0.14	0.02	0.03	0.09	0.00	0.02	0.07	0.03	-0.01	0.32	0.06	0.05	0.04	-0.01	0.01	0.06	0.00	0.02
ROHF	0.01	0.02	-0.01	0.02	0.02	-0.02	0.01	0.02	0.03	-0.03	0.72	0.10	0.09	0.02	-0.01	0.01	0.02	-0.02	0.01
ESMF	0.01	0.03	-0.01	0.02	0.02	-0.02	0.01	0.01	0.03	-0.04	0.71	0.11	0.09	0.03	-0.01	0.00	0.02	-0.02	0.01
CCSD	0.02	0.01	-0.01	0.01	0.01	-0.01	0.00	0.01	0.01	-0.02	0.78	0.09	0.08	0.01	-0.01	0.00	0.01	-0.01	0.00

charge transfer excitation that returns both clusters to charge neutrality.

As seen in Figure 4, the charge density changes predicted by ESMF differ noticeably from those of CIS and  $\omega$ B97X-based<sup>50</sup> TDDFT. Although all three methods (and all others tested, see below) agree that the transferred electron comes from a lone pair on the lower-left water molecule, ESMF also displays two types of significant orbital-relaxation effects that CIS and TDDFT fail to capture. First, electron density in the OH bonds on the affected water molecule is seen to shift towards the oxygen atom, showing a net charge depletion on the hydrogen atoms and some net charge accumulation close to the oxygen atom’s center. Second, the other water molecules show a polarization of their electron densities in response to the newly created hole on the lower-left water. As seen in Table III, these relaxation effects create changes in the Mulliken populations for ESMF that differ significantly from those shown by CIS and TDDFT, both of which predict only significant changes to the lower-left oxygen atom.

At this point, we take advantage of the fact that the two clusters are well separated in order to perform IP/EA-EOM-CCSD<sup>51–53</sup> on the separate clusters in isolation in order to produce a high-level benchmark on what types of charge-relaxation effects other methods should display. As seen in Table III, the coupled cluster predictions for the Mulliken population changes on both the lower-left water and the other water molecules agree reasonably well with the ESMF predictions while disagreeing with the CIS and TDDFT predictions. In particular, CIS and TDDFT fail to predict the significant relaxation near the lower-left water’s hydrogen atoms as well as the degree to which the charge densities on the other water

molecules shift in response to the newly created hole. To verify that these errors are due to the additional approximations (namely a lack of secondary orbital relaxation) associated with CIS and TDDFT as excited state linear-response methods, we have also performed ground state restricted open-shell HF (ROHF) and  $\omega$ B97X-based unrestricted Kohn-Sham (UKS) calculations on the anionic and neutral lower cluster in isolation. As seen in Figure 5 and Table III, these methods both display significant relaxation effects upon creation of the hole on the lower-left water, as should be expected of self-consistent field methods upon the removal of an electron. However, the ROHF and UKS predictions are quite different from each other, with the latter incorrectly delocalizing the hole across all of the water molecules in the lower cluster in a clear display of the difficulties posed by DFT’s self-interaction error, which is known to over-stabilize delocalized states.<sup>54,55</sup> ROHF, ESMF, and coupled cluster, in contrast, are by construction free of self-interaction errors and keep the hole localized on the lower-left water molecule, with the other water molecules showing much smaller net population changes while still correctly shifting their electron clouds to re-polarize after the creation of the hole. Note especially that the ROHF and ESMF results are in close agreement, which is not surprising given that the spin-purity offered by ESMF has only a very small energetic effect in this type of long-range charge transfer excitation. The same logic explains why the ROKS results are very similar to those of UKS, displaying the same clear signs of self-interaction-induced over-delocalization.

As a final note in this system, we remind the reader that ESMF, like HF, should not be expected to deliver highly accurate energetics as it neglects weak correlation effects. For the cluster under study, excitation energy estimates for different methods are shown in Table IV. Note that due to the large system size, we did not pursue a direct EOM-CCSD calculation in the full system. Instead, we created an estimate of the coupled cluster excitation energy via the expression

$$\Delta E = [\text{EA}]_{\text{upper}} - [\text{IP}]_{\text{lower}} + 1/R \quad (17)$$

in which  $[\text{EA}]_{\text{upper}}$  is the electron affinity of the upper cluster in isolation and  $[\text{IP}]_{\text{lower}}$  is the ionization potential of the lower cluster in isolation, as predicted by IP/EA-EOM-CCSD. The  $1/R$  term is used to estimate the Coulomb attraction of the

TABLE IV: Comparison of excitation energies (eV) for the Li-F system’s charge transfer excitation. See text for details of the the CCSD approach.

Method	Excitation Energy
CIS	8.82
TDDFT/ $\omega$ B97X	6.12
ESMF	5.92
CCSD	6.64

two charged clusters in ground state, with  $R$  computed as the distance between Li and F. As we have seen in many other systems,<sup>31</sup> ESMF appears to underestimate the excitation energy. To reach quantitative energetics, a correlation correction such as the one provided by ESMP2<sup>31</sup> is clearly in order. While the current formulation and implementation of that theory is too expensive to use in a system of this size, work exploring more affordable formulations is ongoing.

#### IV. CONCLUSION

We have presented explicit analytic expressions for the derivatives required for ESMF wave function optimization. Although these expressions are somewhat long winded, the upshot is that the necessary derivatives can be evaluated through nine Fock matrix builds and a collection of (much less expensive) single-particle matrix operations. This formulation allows ESMF to immediately benefit from methods that improve the efficiency of Fock builds, a situation we have exploited via the shell-pair screening strategy in order to construct a thread-parallel ESMF implementation that is multiple orders of magnitude faster than the previous implementation, which relied on automatic differentiation. We then applied our method to study a Li-F charge transfer system in which these atoms were surrounded by minimal water solvation shells. By comparing against IP/EA-EOM-CCSD, we found that ESMF's predictions for how the charge transfer excitation changes the electron cloud were qualitatively more accurate than the predictions of CIS, TDDFT, UKS, or ROKS. In particular, ESMF correctly captured post-excitation orbital relaxation effects and, by virtue of being free of self-interaction errors, did not erroneously delocalize the hole.

Looking forward, these findings point to multiple priorities for further research. First, by giving ESMF access to larger systems, they make the development of an  $N^5$ -scaling post-ESMF perturbation theory (as opposed to the  $N^7$ -scaling of the existing<sup>22</sup> version) even more pressing. Happily, a path forward in this direction has been found and will be published soon.<sup>56</sup> Second, we would expect the recently-introduced density functional extension to ESMF to show similar efficiency improvements upon development of Fock-build-based analytic gradients. Finally, in light of the efficiency offered by the successful generalization of the geometric direct minimization method to excited state orbital optimization,<sup>57</sup> it seems likely that employing our new analytic gradients in a custom-tailored quasi-Newton method would lead to further efficiency gains.

#### ACKNOWLEDGMENTS

This work was supported by the National Science Foundation's CAREER program under Award Number 1848012. L.Z. acknowledges additional support from the Dalton Fellowship at the University of Washington. The Berkeley Research Computing Savio cluster performed the calculations.

- <sup>1</sup>G. D. Scholes, G. R. Fleming, A. Olaya-Castro, and R. van Grondelle, "Lessons from nature about solar light harvesting," *Nat. Chem.* **3**, 763–774 (2011).
- <sup>2</sup>S. Refaely-Abramson, F. H. da Jornada, S. G. Louie, and J. B. Neaton, "Origins of singlet fission in solid pentacene from an ab initio green's function approach," *Phys. Rev. Lett.* **119**, 267401 (2017).
- <sup>3</sup>J. K. Stolarczyk, S. Bhattacharyya, L. Polavarapu, and J. Feldmann, "Challenges and prospects in solar water splitting and CO<sub>2</sub> reduction with inorganic and hybrid nanostructures," *ACS Catal.* **8**, 3602–3635 (2018).
- <sup>4</sup>Q. Wang and K. Domen, "Particulate photocatalysts for light-driven water splitting: Mechanisms, challenges, and design strategies," *Chem. Rev. Article ASAP*.
- <sup>5</sup>K. J. Oosterbaan, A. F. White, and M. Head-Gordon, "Non-orthogonal configuration interaction with single substitutions for the calculation of core-excited states," *J. Chem. Phys.* **149**, 044116 (2018).
- <sup>6</sup>M. L. Vidal, X. Feng, E. Epifanovsky, A. I. Krylov, and S. Coriani, "New and efficient equation-of-motion coupled-cluster framework for core-excited and core-ionized states," *J. Chem. Theory Comput.* **15**, 3117–3133 (2019).
- <sup>7</sup>X. Zheng and L. Cheng, "Performance of delta-coupled-cluster methods for calculations of core-ionization energies of first-row elements," *J. Chem. Theory Comput.* **15**, 4945–4955 (2019).
- <sup>8</sup>K. R. Siefermann, C. D. Pemmaraju, S. Neppel, A. Shavorskiy, A. A. Cordones, J. Vura-Weis, D. S. Slaughter, F. P. Sturm, F. Weise, H. Bluhm, *et al.*, "Atomic-scale perspective of ultrafast charge transfer at a dye-semiconductor interface," *J. Phys. Chem. Lett.* **5**, 2753–2759 (2014).
- <sup>9</sup>P. Chábera, K. S. Kjaer, O. Prakash, A. Honarfar, Y. Liu, L. A. Fredin, T. C. B. Harlang, S. Lidin, J. Uhlig, V. Sundström, R. Lomoth, P. Persson, and K. Wärnmark, "Feii hexa n-heterocyclic carbene complex with a 528 ps metal-to-ligand charge-transfer excited-state lifetime," *J. Phys. Chem. Lett.* **9**, 459–463 (2018).
- <sup>10</sup>M. H. Beck, A. Jäckle, G. A. Worth, and H.-D. Meyer, "The multi-configuration time-dependent Hartree (MCTDH) method: an efficient method for propagating wavepackets of several dimensions," *Phys. Rep.* **324**, 1–105 (2000).
- <sup>11</sup>J. C. Tully, "Perspective: Nonadiabatic dynamics theory," *J. Chem. Phys.* **137**, 22A301 (2012).
- <sup>12</sup>T. Ziegler, M. Seth, M. Krykunov, J. Autschbach, and F. Wang, "On the relation between time-dependent and variational density functional theory approaches for the determination of excitation energies and transition moments," *J. Chem. Phys.* **130**, 154102 (2009).
- <sup>13</sup>J. E. Subotnik, "Communication: Configuration interaction singles has a large systematic bias against charge-transfer states," *J. Chem. Phys.* **135**, 071104 (2011).
- <sup>14</sup>Y. C. Park, M. Krykunov, and T. Ziegler, "On the relation between adiabatic time dependent density functional theory (TDDFT) and the  $\Delta$  SCF-DFT method. introducing a numerically stable  $\Delta$  SCF-DFT scheme for local functionals based on constricted variational DFT," *Mol. Phys.* **113**, 1636–1647 (2015).
- <sup>15</sup>L. Zhao and E. Neuscamman, "Density functional extension to excited-state mean-field theory," *J. Chem. Theory Comput.* **16**, 164 (2020).
- <sup>16</sup>A. Dreuw and M. Head-gordon, "Single-Reference ab Initio Methods for the Calculation of Excited States of Large Molecules," *Sciences-New York*, 4009–4037 (2005).
- <sup>17</sup>S. Hirata, M. Head-Gordon, and R. J. Bartlett, "Configuration interaction singles, time-dependent Hartree-Fock, and time-dependent density functional theory for the electronic excited states of extended systems," *J. Chem. Phys.* **111**, 10774–10786 (1999).
- <sup>18</sup>K. Burke, J. Werschnik, and E. K. U. Gross, "Time-dependent density functional theory: Past, present, and future," *J. Chem. Phys.* **123**, 062206 (2005).
- <sup>19</sup>A. I. Krylov, "Equation-of-motion coupled-cluster methods for open-shell and electronically excited species: the Hitchhiker's guide to Fock space," *Annu. Rev. Phys. Chem.* **59**, 433–462 (2008).
- <sup>20</sup>J. D. Watts, S. R. Gwaltney, and R. J. Bartlett, "Coupled-cluster calculations of the excitation energies of ethylene, butadiene, and cyclopentadiene," *J. Chem. Phys.* **105**, 6979–6988 (1996).
- <sup>21</sup>L. Zhao and E. Neuscamman, "An Efficient Variational Principle for the Direct Optimization of Excited States," *J. Chem. Theory Comput.* **12**, 3436–3440 (2016), arXiv:1508.06683.



- <sup>22</sup>J. A. R. Shea and E. Neuscamman, "Communication: A mean field platform for excited state quantum chemistry," *J. Chem. Phys.* **149** (2018).
- <sup>23</sup>P. S. Bagus, "Self-consistent-field wave functions for hole states of some ne-like and ar-like ions," *Phys. Rev.* **139**, A619 (1965).
- <sup>24</sup>H.-I. Hsu, E. R. Davidson, and R. M. Pitzer, "An scf method for hole states," *J. Chem. Phys.* **65**, 609–613 (1976).
- <sup>25</sup>A. Naves de Brito, N. Correia, S. Svensson, and H. Ågren, "A theoretical study of x-ray photoelectron spectra of model molecules for polymethylmethacrylate," *J. Chem. Phys.* **95**, 2965–2974 (1991).
- <sup>26</sup>N. A. Besley, A. T. Gilbert, and P. M. Gill, "Self-consistent-field calculations of core excited states," *J. Chem. Phys.* **130**, 124308 (2009).
- <sup>27</sup>M. Filatov and S. Shaik, "A spin-restricted ensemble-referenced kohn-sham method and its application to diradicaloid situations," *Chem. Phys. Lett.* **304**, 429–437 (1999).
- <sup>28</sup>T. Kowalczyk, T. Tsuchimochi, P. T. Chen, L. Top, and T. Van Voorhis, "Excitation energies and Stokes shifts from a restricted open-shell Kohn-Sham approach," *J. Chem. Phys.* **138** (2013).
- <sup>29</sup>A. Szabo and N. S. Ostlund, *Modern Quantum Chemistry: Introduction to Advanced Electronic Structure Theory* (Dover Publications, Mineola, N.Y., 1996).
- <sup>30</sup>T. Helgaker, P. Jørgensen, and J. Olsen, *Molecular Electronic Structure Theory* (John Wiley and Sons, Ltd, West Sussex, England, 2000) p. 162.
- <sup>31</sup>J. A. R. Shea, E. Gwin, and E. Neuscamman, "A generalized variational principle with applications to excited state mean field theory," *arXiv*, 1910.03145 (2019).
- <sup>32</sup>H.-Z. Ye, M. Welborn, N. D. Rieke, and T. Van Voorhis, " $\sigma$ -scf: A direct energy-targeting method to mean-field excited states," *J. Chem. Phys.* **147**, 214104 (2017).
- <sup>33</sup>H. Ye and T. V. Voorhis, "Half-projected  $\sigma$  self-consistent field for electronic excited states," *J. Chem. Theory Comput.* **15**(5), 2954–2964 (2019).
- <sup>34</sup>C. Umrigar, K. Wilson, and J. Wilkins, "Optimized trial wave functions for quantum monte carlo calculations," *Phys. Rev. Lett.* **60**, 1719 (1988).
- <sup>35</sup>J. A. R. Shea and E. Neuscamman, "Size consistent excited states via algorithmic transformations between variational principles," *J. Chem. Theory Comput.* **13**, 6078–6088 (2017).
- <sup>36</sup>S. D. Pineda Flores and E. Neuscamman, "Excited state specific multi-slater jastrow wave functions," *J. Phys. Chem. A* **123**, 1487–1497 (2019).
- <sup>37</sup>M. Abadi, A. Agarwal, P. Barham, E. Brevdo, Z. Chen, C. Citro, G. S. Corrado, A. Davis, J. Dean, M. Devin, S. Ghemawat, I. Goodfellow, A. Harp, G. Irving, M. Isard, Y. Jia, R. Jozefowicz, L. Kaiser, M. Kudlur, J. Levenberg, D. Mané, R. Monga, S. Moore, D. Murray, C. Olah, M. Schuster, J. Shlens, B. Steiner, I. Sutskever, K. Talwar, P. Tucker, V. Vanhoucke, V. Vasudevan, F. Viégas, O. Vinyals, P. Warden, M. Wattenberg, M. Wicke, Y. Yu, and X. Zheng, "TensorFlow: Large-scale machine learning on heterogeneous systems," (2015), software available from tensorflow.org.
- <sup>38</sup>D. S. Lambrecht, B. Doser, and C. Ochsenfeld, "Rigorous integral screening for electron correlation methods," *J. Chem. Phys.* **123**, 184102 (2005).
- <sup>39</sup>A. Sodt, J. E. Subotnik, and M. Head-Gordon, "Linear scaling density fitting," *J. Chem. Phys.* **125**, 194109 (2006).
- <sup>40</sup>E. G. Hohenstein, R. M. Parrish, and T. J. Martínez, "Tensor hypercontraction density fitting. I. Quartic scaling second- and third-order Møller-Plesset perturbation theory," *J. Chem. Phys.* **137**, 044103 (2012).
- <sup>41</sup>R. M. Parrish, E. G. Hohenstein, T. J. Martínez, and C. D. Sherrill, "Tensor hypercontraction. II. Least-squares renormalization," *J. Chem. Phys.* **137**, 224106 (2012).
- <sup>42</sup>E. G. Hohenstein, R. M. Parrish, C. D. Sherrill, and T. J. Martínez, "Communication: Tensor hypercontraction. III. Least-squares tensor hypercontraction for the determination of correlated wavefunctions," *J. Chem. Phys.* **137**, 221101 (2012).
- <sup>43</sup>Q. Sun, T. C. Berkelbach, N. S. Blunt, G. H. Booth, S. Guo, Z. Li, J. Liu, J. D. McClain, E. R. Sayfutyarova, S. Sharma, S. Wouters, and G. K. L. Chan, "PySCF: the Python-based simulations of chemistry framework," *Wiley Interdiscip. Rev. Comput. Mol. Sci.* **8** (2018).
- <sup>44</sup>Y. Shao, Z. Gan, E. Epifanovsky, A. T. Gilbert, M. Wormit, J. Kussmann, A. W. Lange, A. Behn, J. Deng, X. Feng, D. Ghosh, M. Goldey, P. R. Horn, L. D. Jacobson, I. Kaliman, R. Z. Khaliullin, T. Kuš, A. Landau, J. Liu, E. I. Proynov, Y. M. Rhee, R. M. Richard, M. A. Rohrdanz, R. P. Steele, E. J. Sundstrom, H. L. W. III, P. M. Zimmerman, D. Zuev, B. Albrecht, E. Alguire, B. Austin, G. J. O. Beran, Y. A. Bernard, E. Berquist, K. Brandhorst, K. B. Bravaya, S. T. Brown, D. Casanova, C.-M. Chang, Y. Chen, S. H. Chien, K. D. Closser, D. L. Crittenden, M. Diedenhofen, R. A. D. Jr., H. Do, A. D. Dutoi, R. G. Edgar, S. Fatehi, L. Fusti-Molnar, A. Ghysels, A. Golubeva-Zadorozhnaya, J. Gomes, M. W. Hanson-Heine, P. H. Harbach, A. W. Hauser, E. G. Hohenstein, Z. C. Holden, T.-C. Jagau, H. Ji, B. Kaduk, K. Khistyayev, J. Kim, J. Kim, R. A. King, P. Klunzinger, D. Kosenkov, T. Kowalczyk, C. M. Krauter, K. U. Lao, A. D. Laurrent, K. V. Lawler, S. V. Levchenko, C. Y. Lin, F. Liu, E. Livshits, R. C. Lochan, A. Luenser, P. Manohar, S. F. Manzer, S.-P. Mao, N. Mardirossian, A. V. Marenich, S. A. Maurer, N. J. Mayhall, E. Neuscamman, C. M. Oana, R. Olivares-Amaya, D. P. O'Neill, J. A. Parkhill, T. M. Perrine, R. Peverati, A. Prociuk, D. R. Rehn, E. Rosta, N. J. Russ, S. M. Sharada, S. Sharma, D. W. Small, A. Sodt, T. Stein, D. Stück, Y.-C. Su, A. J. Thom, T. Tsuchimochi, V. Vanovschi, L. Vogt, O. Vydrov, T. Wang, M. A. Watson, J. Wenzel, A. White, C. F. Williams, J. Yang, S. Yeganeh, S. R. Yost, Z.-Q. You, I. Y. Zhang, X. Zhang, Y. Zhao, B. R. Brooks, G. K. Chan, D. M. Chipman, C. J. Cramer, W. A. G. III, M. S. Gordon, W. J. Hehre, A. Klamt, H. F. S. III, M. W. Schmidt, C. D. Sherrill, D. G. Truhlar, A. Warshel, X. Xu, A. Aspuru-Guzik, R. Baer, A. T. Bell, N. A. Besley, J.-D. Chai, A. Dreuw, B. D. Dunietz, T. R. Furlani, S. R. Gwaltney, C.-P. Hsu, Y. Jung, J. Kong, D. S. Lambrecht, W. Liang, C. Ochsenfeld, V. A. Rassolov, L. V. Slipchenko, J. E. Subotnik, T. V. Voorhis, J. M. Herbert, A. I. Krylov, P. M. Gill, and M. Head-Gordon, "Advances in molecular quantum chemistry contained in the q-chem 4 program package," *Mol. Phys.* **113**, 184–215 (2015).
- <sup>45</sup>K. Momma and F. Izumi, "Vesta 3 for three-dimensional visualization of crystal, volumetric and morphology data," *J. Appl. Cryst.* **44**, 1272–1276 (2011).
- <sup>46</sup>T. H. Dunning, "Gaussian basis sets for use in correlated molecular calculations. I. the atoms boron through neon and hydrogen," *J. Chem. Phys.* **90**, 1007 (1988).
- <sup>47</sup>Y. Zhao and D. G. Truhlar, "Density functional for spectroscopy: No long-range self-interaction error, good performance for Rydberg and charge-transfer states, and better performance on average than B3LYP for ground states," *J. Phys. Chem. A* **110**, 13126–13130 (2006).
- <sup>48</sup>D. Majumdar, J. Kim, and K. S. Kim, "Charge transfer to solvent (CTTS) energies of small  $X^-(H_2O)_{n=1-4}$  ( $X = F, Cl, Br, I$ ) clusters: Ab initio study," *J. Chem. Phys.* **112**, 101 (2000).
- <sup>49</sup>G. A. Petersson, A. Bennett, T. G. Tensfeldt, M. A. Al-Laham, W. A. Shirley, and J. Mantzaris, "A complete basis set model chemistry. i. the total energies of closed-shell atoms and hydrides of the first-row atoms," *J. Chem. Phys.* **89**, 2193–218 (1988).
- <sup>50</sup>J.-D. Chai and M. Head-Gordon, "Systematic optimization of long-range corrected hybrid density functionals," *J. Chem. Phys.* **128**, 084106 (2008).
- <sup>51</sup>D. Sinha, S. K. Mukhopadhyay, R. Chaudhuri, and D. Mukherjee, "The eigenvalue-independent partitioning technique in fock space: An alternative route to open-shell coupled-cluster theory for incomplete model spaces," *Chem. Phys. Lett.* **164**, 544 (1988).
- <sup>52</sup>J. F. Stanton and J. Gauss, "Analytic energy derivatives for ionized states described by the equation-of-motion coupled cluster method," *J. Chem. Phys.* **1010**, 8938 (1994).
- <sup>53</sup>M. Nooijen and R. J. Barlett, "Equation of motion coupled cluster method for electron attachment," *J. Chem. Phys.* **102**, 3629 (1995).
- <sup>54</sup>M. Lundberg and P. E. Siegbahn, "Quantifying the effects of the self-interaction error in DFT: When do the delocalized states appear?" *J. Chem. Phys.* **122**, 224103 (2005).
- <sup>55</sup>A. J. Cohen, P. Mori-Sánchez, and W. Yang, "Insights into Current Limitations of Density Functional Theory," *Science* **321**, 792–794 (2008).
- <sup>56</sup>R. Clune, J. A. R. Shea, and E. Neuscamman, in preparation.
- <sup>57</sup>D. Hait and M. Head-Gordon, "Excited state orbital optimization via minimizing the square of the gradient: General approach and application to singly and doubly excited states via density functional theory," *arXiv:1911.04709* (2019).

## Appendix A: Molecular Geometries

The geometry of Cl-H<sub>2</sub>O is, (units are in Å)

Cl	-0.848210	0.000015	0.074343
O	2.337083	0.000017	0.186525

H	1.693454	0.725249	0.163751
H	1.693562	-0.725306	0.163748
The geometry of NH <sub>3</sub> -F <sub>2</sub> is,			
N	0.000000	0.000000	6.000000
H	0.000000	0.939731	5.611703
H	0.813831	-0.469865	5.611703
H	-0.813831	-0.469865	5.611703
F	0.000000	0.000000	12.000000
F	0.000000	0.000000	13.430000

The geometry of Li-F system is, (units are in Å)

Li	1.796944	0.402653	7.714191
O	0.913870	1.932310	6.845200
O	0.377075	-0.964195	7.698416
O	2.515306	0.844431	9.484318
O	3.091745	-0.174192	6.348637
H	3.349025	0.540540	9.879509
H	2.133055	1.467664	10.123912
H	3.887425	-0.730479	6.379252
H	3.192501	0.388996	5.562935
H	0.429815	-1.696650	7.061571
H	-0.089280	-1.321908	8.472304
H	1.105006	2.884390	6.866262
H	-0.019955	1.852997	6.587612
F	0.243106	-0.058090	-0.170912
O	2.303862	1.382309	0.978656
O	-2.282249	-0.646317	-1.078369
O	0.137241	2.682825	-0.515020
O	2.626535	-0.051411	-1.623087
O	-1.783124	1.055466	1.206736
O	-1.154603	-1.907153	1.277859
H	1.641197	0.687837	0.777891
H	1.835652	2.163873	0.627908
H	-1.334445	-0.386089	-1.061835
H	-2.258393	-1.373147	-0.426111
H	-0.447054	-1.443480	0.773265
H	-1.562261	-1.153285	1.740562
H	2.944434	0.519587	-0.901516
H	1.727649	-0.252872	-1.297097
H	-0.614192	2.646830	0.104027
H	0.260635	1.727937	-0.704091
H	-0.914261	0.722919	0.879951
H	-2.352180	0.731683	0.478898

## Appendix B: Analytical Derivatives of ESMF Energy and Target Function

From the ESMF energy, we could compute its first order derivatives. The derivative with respect to  $c_0$  is,

$$\begin{aligned} \frac{\partial E}{\partial c_0} = & (4c_0 \text{Tr}[\Theta \mathbf{G} \Theta^T] + 4\text{Tr}[\Theta \mathbf{G} \Gamma^T \sigma^T] \\ & + 2c_0 \mathbf{F}[\Theta^T \Theta] \cdot (\Theta^T \Theta) + 4\mathbf{F}[\Theta^T \Theta] \cdot (\Theta^T \sigma \Gamma)) / N_2 \\ & - 2c_0 E / N_2 \end{aligned} \quad (\text{B1})$$

The derivative with respect to  $\sigma_{jb}$  is,

$$\begin{aligned} \frac{\partial E}{\partial \sigma_{jb}} = & \left( 4c_0 (\Theta \mathbf{G} \Gamma^T)_{jb} + 4(\sigma \Gamma \mathbf{G} \Gamma^T)_{jb} \right. \\ & - 4(\Theta \mathbf{G} \Theta^T \sigma)_{jb} + 8\text{Tr}[\Theta \mathbf{G} \Theta^T] \sigma_{jb} \\ & + 4c_0 (\Theta \mathbf{F}[\Theta^T \Theta] \Gamma^T)_{jb} + 4(\sigma \Gamma \mathbf{F}[\Theta^T \Theta] \Gamma^T)_{jb} \\ & - 4(\Theta \mathbf{F}[\Theta^T \Theta] \Theta^T \sigma)_{jb} + 4(\Theta \mathbf{F}[\Theta^T \sigma \Gamma] \Gamma^T)_{jb} \\ & \left. + 4 \sum_{pq} (\mathbf{F}[\Theta^T \Theta] \Theta^T \Theta)_{pq} \sigma_{jb} \right) / N_2 \\ & - 4E \sigma_{jb} / N_2 \end{aligned} \quad (\text{B2})$$

The derivative with respect to  $\Theta_{kp}$  is,

$$\begin{aligned} \frac{\partial E}{\partial \Theta_{kp}} = & \left( 4N_2 (\Theta \mathbf{G})_{kp} + 4c_0 (\sigma \Gamma \mathbf{G})_{kp} \right. \\ & - 4(\sigma \sigma^T \Theta \mathbf{G})_{kp} + 4N_2 (\Theta \mathbf{F}[\Theta^T \Theta])_{kp} \\ & + 4c_0 (\sigma \Gamma \mathbf{F}[\Theta^T \sigma \Gamma])_{kp} \\ & + 4c_0 (\Theta (\mathbf{F}[\Theta^T \sigma \Gamma] - \mathbf{F}[\Theta^T \sigma \Gamma]^T))_{kp} \\ & + 2(\Theta (\mathbf{F}[\mathbf{A}] - \mathbf{F}[\mathbf{A}]^T))_{kp} - 4(\sigma \sigma^T \Theta \mathbf{F}[\Theta^T \Theta])_{kp} \\ & \left. + 4(\sigma \Gamma \mathbf{F}[\Theta^T \sigma \Gamma])_{kp} / N_2 \right) \end{aligned} \quad (\text{B3})$$

The derivative with respect to  $\Gamma_{cp}$  is,

$$\begin{aligned} \frac{\partial E}{\partial \Gamma_{cp}} = & \left( 4c_0 (\sigma^T \Theta \mathbf{G})_{cp} + 4(\sigma^T \sigma \Gamma \mathbf{G})_{cp} \right. \\ & + 4c_0 (\sigma^T \Theta \mathbf{F}[\Theta^T \Theta])_{cp} + 4(\sigma^T \sigma \Gamma \mathbf{F}[\Theta^T \Theta])_{cp} \\ & \left. + 4(\sigma^T \Theta \mathbf{F}[\Theta^T \sigma \Gamma])_{cp} \right) \end{aligned} \quad (\text{B4})$$

Let us now define different pieces of L,

The derivatives of  $L_1$ ,  $L_2$ , and  $L_3$  with respect to  $\sigma_{jb}$  are,

$$\begin{aligned}
L_1 &= 4c_0 \text{Tr}[\Theta \mathbf{G} \Theta^T] + 4 \text{Tr}[\Theta \mathbf{G} \Gamma^T \sigma^T] \\
&\quad + 2c_0 F[\Theta^T \Theta] \cdot (\Theta^T \Theta) + 4F[\Theta^T \Theta] \cdot (\Theta^T \sigma \Gamma) \\
L_2 &= 4c_0 \text{Tr}[\Theta \mathbf{G} \Gamma^T \mu^T] + 4 \text{Tr}[\sigma \Gamma \mathbf{G} \Gamma^T \mu^T] \\
&\quad - 2 \text{Tr}[\Theta \mathbf{G} \Theta^T \sigma \mu^T + \Theta \mathbf{G} \Theta^T \mu \sigma^T] + 8 \sigma \cdot \mu \text{Tr}[\Theta \mathbf{G} \Theta^T] \\
&\quad + 4c_0 F[\Theta^T \Theta] \cdot (\Theta^T \mu \Gamma) \\
&\quad + 2F[\Theta^T \Theta] \cdot (\Gamma^T \sigma^T \mu \Gamma + \Gamma^T \mu^T \sigma \Gamma - \Theta^T \mu \sigma^T \Theta - \Theta^T \sigma \mu^T \Theta) \\
&\quad + 4(\sigma \cdot \mu) (F[\Theta^T \Theta] \cdot (\Theta^T \Theta)) + 4F[\Theta^T \sigma \Gamma] \cdot (\Theta^T \sigma \Gamma) \\
L_3 &= 4N_2 \text{Tr}[\mathbf{R} \mathbf{G} \Theta^T] + 4c_0 \text{Tr}[\mathbf{R} \mathbf{G} \Gamma^T \sigma^T] \\
&\quad - 2 \text{Tr}[\mathbf{R} \mathbf{G} \Theta^T \sigma \sigma^T + \Theta \mathbf{G} \mathbf{R}^T \sigma \sigma^T] \\
&\quad + 2N_2 (F[\mathbf{R}^T \Theta] + F[\mathbf{R}^T \Theta]^T) \cdot (\Theta^T \Theta) \\
&\quad + 4c_0 (F[\mathbf{R}^T \Theta] + F[\mathbf{R}^T \Theta]^T) \cdot (\Theta^T \sigma \Gamma) \\
&\quad + 4c_0 F[\Theta^T \Theta] \cdot (\mathbf{R}^T \sigma \Gamma) \\
&\quad + 2(F[\mathbf{R}^T \Theta] + F[\mathbf{R}^T \Theta]^T) \cdot \mathbf{A} \\
&\quad - 2F[\Theta^T \Theta] \cdot (\mathbf{R}^T \sigma \sigma^T \Theta + (\mathbf{R}^T \sigma \sigma^T \Theta)^T) \\
&\quad + 4F[\mathbf{R}^T \sigma \Gamma] \cdot (\Theta^T \sigma \Gamma) \\
&\quad + 4c_0 \text{Tr}[\Theta \mathbf{G} \Phi^T \sigma^T] + 2 \text{Tr}[\sigma \Gamma \mathbf{G} \Phi^T \sigma^T + (\sigma \Gamma \mathbf{G} \Phi^T \sigma^T)^T] \\
&\quad + 4c_0 F[\Theta^T \Theta] \cdot (\Theta^T \sigma \Phi) \\
&\quad + 2F[\Theta^T \Theta] \cdot (\Phi^T \sigma^T \sigma \Gamma + (\Phi^T \sigma^T \sigma \Gamma)^T) \\
&\quad + 4F[\Theta^T \sigma \Gamma] \cdot (\Theta^T \sigma \Phi)
\end{aligned} \tag{B5}$$

The derivatives of  $L_1$ ,  $L_2$ , and  $L_3$  with respect to  $c_0$  are,

$$\begin{aligned}
\frac{\partial L_1}{\partial c_0} &= 4 \text{Tr}[\Theta \mathbf{G} \Theta^T] + 2F[\Theta^T \Theta] \cdot (\Theta^T \Theta) \\
\frac{\partial L_2}{\partial c_0} &= 4 \text{Tr}[\Theta \mathbf{G} \Gamma^T \mu^T] + 4F[\Theta^T \Theta] \cdot (\Theta^T \mu \Gamma) \\
\frac{\partial L_3}{\partial c_0} &= 8c_0 \text{Tr}[\mathbf{R} \mathbf{G} \Theta^T] + 4 \text{Tr}[\mathbf{R} \mathbf{G} \Gamma^T \sigma^T] \\
&\quad + 4c_0 (F[\mathbf{R}^T \Theta] + F[\mathbf{R}^T \Theta]^T) \cdot (\Theta^T \sigma \Gamma) \\
&\quad + 4F[\Theta^T \Theta] \cdot (\mathbf{R}^T \sigma \Gamma) \\
&\quad + 4 \text{Tr}[\Theta \mathbf{G} \Phi^T \sigma^T] + 4F[\Theta^T \Theta] \cdot (\Theta^T \sigma \Phi)
\end{aligned} \tag{B6}$$

in which no new Fock build is needed.

$$\begin{aligned}
\frac{\partial L_1}{\partial \sigma_{jb}} &= 4(\Theta \mathbf{G} \Gamma^T)_{jb} + 4(\Theta F[\Theta^T \Theta] \Gamma^T)_{jb} \\
\frac{\partial L_2}{\partial \sigma_{jb}} &= 4(\Gamma \mathbf{G} \Gamma^T \mu^T)_{jb}^T - 4(\Theta \mathbf{G} \Theta^T \mu)_{jb} + 8 \text{Tr}[\Theta \mathbf{G} \Theta^T] \mu_{jb} \\
&\quad + 2(\mu \Gamma (F[\Theta^T \Theta] + F[\Theta^T \Theta]^T) \Gamma^T)_{jb} \\
&\quad - 2(\Theta (F[\Theta^T \Theta] + F[\Theta^T \Theta]^T) \Theta^T \mu)_{jb} \\
&\quad + 4F[\Theta^T \Theta] \cdot (\Theta^T \Theta) \mu_{jb} + 4(\Theta F[\Theta^T \mu \Gamma] \Gamma^T)_{jb} \\
\frac{\partial L_3}{\partial \sigma_{jb}} &= 4c_0 (\mathbf{R} \mathbf{G} \Gamma^T)_{jb} - 4(\mathbf{R} \mathbf{G} \Theta^T \sigma)_{jb} + 16 \text{Tr}[\mathbf{R} \mathbf{G} \Theta^T] \sigma_{jb} \\
&\quad + 4c_0 (\Theta (F[\mathbf{R}^T \Theta] + F[\mathbf{R}^T \Theta]^T) \Gamma^T)_{jb} \\
&\quad + 4(\sigma \Gamma (F[\mathbf{R}^T \Theta] + F[\mathbf{R}^T \Theta]^T) \Gamma^T)_{jb} \\
&\quad - 4(\Theta (F[\mathbf{R}^T \Theta] + F[\mathbf{R}^T \Theta]^T) \Theta^T \sigma)_{jb} \\
&\quad + 4c_0 (\mathbf{R} F[\Theta^T \Theta] \Gamma^T)_{jb} \\
&\quad - 2(\mathbf{R} (F[\Theta^T \Theta] + F[\Theta^T \Theta]^T) \Theta^T \sigma)_{jb} \\
&\quad - 2(\Theta (F[\Theta^T \Theta] + F[\Theta^T \Theta]^T) \mathbf{R}^T \sigma)_{jb} \\
&\quad + 4(\mathbf{R} F[\Theta^T \sigma \Gamma] \mathbf{U}^T)_{jb} + 4(\Theta F[\mathbf{R}^T \sigma \Gamma] \Gamma^T)_{jb} \\
&\quad + 8F[\Theta^T \Theta] \cdot (R^T \Theta + \Theta R^T) \sigma_{jb} \\
&\quad + 4c_0 (\Phi \mathbf{G} \Theta^T)_{jb}^T + 4(\Phi \mathbf{G} \Gamma^T \sigma^T)_{jb}^T + 4(\Gamma \mathbf{G} \Phi^T \sigma^T)_{jb}^T \\
&\quad + 4c_0 (\Theta F[\Theta^T \Theta] \Phi^T)_{jb} \\
&\quad + 2(\sigma \Phi (F[\Theta^T \Theta] + F[\Theta^T \Theta]^T) \Gamma^T)_{jb} \\
&\quad + 2(\sigma \Gamma (F[\Theta^T \Theta] + F[\Theta^T \Theta]^T) \Phi^T)_{jb} \\
&\quad + 4(\Theta (F[\Theta^T \sigma \Gamma] + F[\Theta^T \sigma \Gamma]^T) \Phi^T)_{jb} \\
&\quad + 4(\Theta (F[\Theta^T \sigma \Phi] + F[\Theta^T \sigma \Phi]^T) \Gamma^T)_{jb}
\end{aligned} \tag{B7}$$

(B7)

The derivatives of  $L_1$ ,  $L_2$ , and  $L_3$  with respect to  $\Theta_{kp}$  are,

$$\begin{aligned}
\frac{\partial L_1}{\partial \Theta_{kp}} &= 8c_0 (\Theta G)_{kp} + 4 (\sigma \Gamma G)_{kp} \\
&\quad + 8c_0 (\Theta F [\Theta^T \Theta])_{kp} + 4 (\sigma \Gamma F [\Theta^T \Theta])_{kp} \\
&\quad + 4 (\Theta (F [\Theta^T \sigma \Gamma] + F [\Theta^T \sigma \Gamma]^T))_{kp} \\
\frac{\partial L_2}{\partial \Theta_{kp}} &= 4c_0 (\mu \Gamma G)_{kp} - 4 (\mu \sigma^T \Theta G)_{kp} + 16\sigma \cdot \mu (\Theta G)_{kp} \\
&\quad + 4c_0 (\mu \Gamma F [\Theta^T \Theta]^T)_{kp} \\
&\quad + 4c_0 (\Theta (F [\Theta^T \mu \Gamma] + F [\Theta^T \mu \Gamma]^T))_{kp} \\
&\quad - 4 (\Theta (F [\Theta^T \mu \sigma^T \Theta] + F [\Theta^T \mu \sigma^T \Theta]^T))_{kp} \\
&\quad - 2 ((\mu \sigma^T \Theta + \sigma \mu^T \Theta) (F [\Theta^T \Theta] + F [\Theta^T \Theta]^T))_{kp} \\
&\quad + 8\sigma \cdot \mu (\Theta (F [\Theta^T \Theta] + F [\Theta^T \Theta]^T))_{kp} \\
&\quad + 4 (\mu \Gamma F [\Theta^T \sigma \Gamma]^T)_{kp} + 4 (\sigma \Gamma F [\Theta^T \mu \Gamma]^T)_{kp} \\
\frac{\partial L_3}{\partial \Theta_{kp}} &= 4N_2 (RG)_{kp} - 4 (\sigma \sigma^T RG)_{kp} \\
&\quad + 2N_2 (R (F [\Theta^T \Theta] + F [\Theta^T \Theta]^T))_{kp} \\
&\quad + 4N_2 (\Theta (F [R^T \Theta] + F [R^T \Theta]^T))_{kp} \\
&\quad + 4c_0 (R (F [\Theta^T \sigma \Gamma] + F [\Theta^T \sigma \Gamma]^T))_{kp} \\
&\quad + 4c_0 (\sigma \Gamma (F [R^T \Theta] + F [R^T \Theta]^T))_{kp} \\
&\quad + 4c_0 (\Theta (F [R^T \sigma \Gamma] + F [R^T \sigma \Gamma]^T))_{kp} \\
&\quad + 4c_0 (\Theta (F [\Theta^T \sigma \Phi] + F [\Theta^T \sigma \Phi]^T))_{kp} \\
&\quad + 4c_0 (\sigma \Phi F [\Theta^T \Theta])_{kp} + 2 (R (F [A] + F [A]^T))_{kp} \\
&\quad - 4 (\sigma \sigma^T \Theta (F [R^T \Theta] + F [R^T \Theta]^T))_{kp} \\
&\quad + 4 (\Theta (F [B] + F [B]^T))_{kp} \\
&\quad - 2 (\sigma \sigma^T R (F [\Theta^T \Theta] + F [\Theta^T \Theta]^T))_{kp} \\
&\quad + 4 (\sigma \Gamma F [R^T \sigma \Gamma]^T)_{kp} \\
&\quad + 4 (\sigma \Phi F [\Theta^T \sigma \Gamma]^T)_{kp} \\
&\quad + 4 (\sigma \Gamma F [\Theta^T \sigma \Phi]^T)_{kp}
\end{aligned}$$

(B8)

The derivatives of  $L_1$ ,  $L_2$ , and  $L_3$  with respect to  $\Gamma_{cp}$  are,

$$\begin{aligned}
\frac{\partial L_1}{\partial \Gamma_{cp}} &= 4 (\sigma^T \Theta G)_{cp} + 4 (\sigma^T \Theta F [\Theta^T \Theta])_{cp} \\
\frac{\partial L_2}{\partial \Gamma_{cp}} &= 4c_0 (\mu \Gamma G)_{cp} - 4 (\mu \sigma^T \Theta G)_{cp} \\
&\quad + 4 (\sigma^T \mu \Gamma G)_{cp} + 4c_0 (\mu^T \Theta F [\Theta^T \Theta])_{cp} \\
&\quad + 2 (\sigma^T \mu \Gamma (F [\Theta^T \Theta] + F [\Theta^T \Theta]^T))_{cp} \\
&\quad + 2 (\mu^T \sigma \Gamma (F [\Theta^T \Theta] + F [\Theta^T \Theta]^T))_{cp} \\
&\quad + 4 (\sigma^T \Theta F [\Theta^T \mu \Gamma])_{cp} + 4 (\mu^T \Theta F [\Theta^T \sigma \Gamma])_{cp} \\
\frac{\partial L_3}{\partial \Gamma_{cp}} &= 4c_0 (\sigma^T RG)_{cp} + 4 (\sigma^T \sigma \Phi G)_{cp} \tag{B9} \\
&\quad + 4c_0 (\sigma^T \Theta (F [R^T \Theta] + F [R^T \Theta]^T))_{cp} \\
&\quad + 4 (\sigma^T \sigma \Gamma (F [R^T \Theta] + F [R^T \Theta]^T))_{cp} \\
&\quad + 4c_0 (\sigma^T R F [\Theta^T \Theta])_{cp} \\
&\quad + 4 (\sigma^T R F [\Theta^T \sigma \Gamma])_{cp} \\
&\quad + 4 (\sigma^T \Theta F [R^T \sigma \Gamma])_{cp} \\
&\quad + 2 (\sigma^T \sigma \Phi (F [\Theta^T \Theta] + F [\Theta^T \Theta]^T))_{cp} \\
&\quad + 4 (\sigma^T \Theta F [\Theta^T \sigma \Phi])_{cp}
\end{aligned}$$

### Appendix C: Isosurface Plots

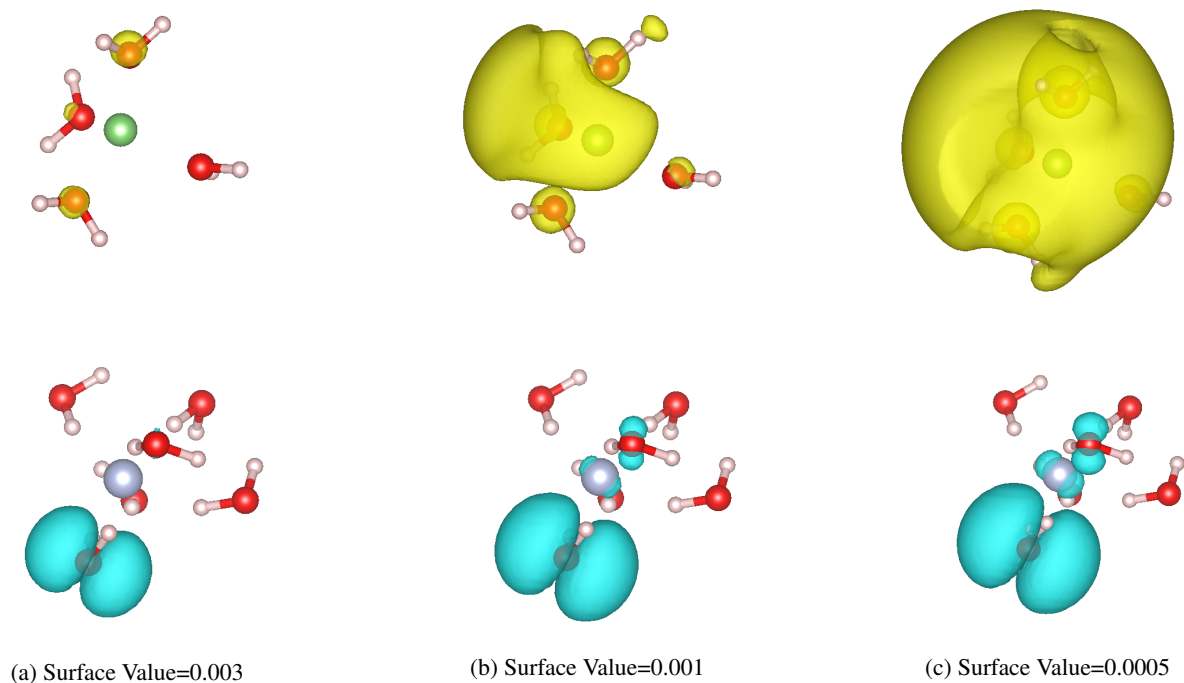


FIG. 6: CIS isosurface plots with different thresholds for the charge density changes following the charge transfer excitation that moves an electron from the lower F cluster to the upper Li cluster, with blue surfaces showing charge depletion relative to the ground state and yellow surfaces showing charge accumulation.